DOI: 10.13009/EUCASS2022-4925
9TH EUROPEAN CONFERENCE FOR AERONAUTICS AND SPACE SCIENCES (EUCASS)

Heat flux characterization of an under-expanded/supersonic plasma jet over a catalytic probe

Michele Capriati[⋆§†]*, Alessandro Turchi*[⋆]*, Pietro M. Congedo*[§]*, and Thierry E. Magin*[⋆]

[⋆] *von Karman Institute for Fluid Dynamics*
Waterloosesteenweg 72, 1640 Sint-Genesius-Rode (BE)
[§] *Inria, Centre de Mathematiques Appliquees, Ecole Polytechnique, IPP*
Route de Saclay, 91120 Palaiseau (FR)
[†] Corresponding author
michele.capriati@vki.ac.be ·

June 10, 2022

Abstract

Supersonic plasma testing allows to achieve high heat flux and, in the case of ablative samples, non-uniform recession. We propose a methodology to characterize the flow. Experimental and modeling uncertainties are propagated through a surrogate model to estimate the variability of the quantities of interest. The high computational cost demanded by the CFD computations, needed to train the surrogate model, is lowered by employing a multi-fidelity formulation. The work shows that is possible to build a reliable surrogate model using few high fidelity computations. The propagated numerical uncertainties partially overlaps with the experimental ones for all the quantities of interest.

1. Introduction

The von Karman Institute (VKI) Inductively-Coupled Plasma (ICP) Plasmatron facility[6] is widely used for the characterization of materials exposed to a high-enthalpy plasma environment.[13,23,26] It is particularly helpful to predict the behaviour of Thermal Protection Materials (TPMs) for aerospace. In atmospheric entry applications, TPMs protect the vehicle from the extremely demanding aerodynamic conditions to which it is exposed. However, this normally happens at the expenses of the TPM that undergoes thermochemical decomposition and experiences mass loss and shape change.

When the Local Heat Transfer Simulation (LHTS) constraints are met, the in-flight highly chemically reactive boundary layer can be on ground duplicated, in the stagnation point region, by a subsonic plasma flow.[30,45] Anyway, differences still remain in the heat flux and ablation distributions along the body. In particular, contrary to the in-flight non-uniform recession, the one experienced by a typical hemispherical ablative TPM sample exposed to the subsonic plasma flow is almost uniform in space and the shape is preserved.[24]

A supersonic experimental campaign has been recently conducted at the VKI to explore this behaviour. The supersonic condition was achieved by I) mounting a sonic nozzle at the end of the plasma torch, that expands the gas to choked conditions, and II) adequately lowering the chamber pressure, resulting in an under-expanded supersonic jet. A similar configuration was also investigated by Gordeev and Sakharov[18,40] to study the evolution of heat flux and pressure along the jet center line. The resulting thermo-aerodynamic environment over the sample is close to the one produced by arc-jets, as the Interaction Heating Facility (IHF),[2] where the flow is expanded to supersonic condition through a convergent-divergent nozzle.

The Plasmatron test chamber is equipped with probes to measure the static and the dynamic pressure, and the heat flux. A rotameter allows for mass flow rate determination. While a spectrograph may be used to access the boundary edge enthalpy by detecting the radiative signature of atoms or molecules,[14] it is customary to rely on a coupled numerical framework for its estimation.[24,26] In general, this procedure aims in rebuilding the Quantities of Interest (QoIs) that are not accessible by means of the only experimental set-up. In numerically simulating the flow, several assumptions have to be made. First of all, the flow is assumed to be in chemical equilibrium up to the boundary layer edge. The surface catalytic behaviour is also assumed to be well known, even if its efficiency may vary from fully to low catalytic,

DOI: 10.13009/EUCASS2022-4925

depending on the chamber pressure and the presence of surface oxides.[48] Recently, this deterministic rebuilding procedure was investigated in the stochastic space to account for the experimental uncertainties and for the model unknowns by Sanson[41,42] and by del Val.[10,11,46]

Also in supersonic testing the pressure at the nozzle inlet and in the chamber can be experimentally measured, and the enthalpy at the nozzle inlet is not directly measurable and its value needs to be inferred. Anyway, differently from the subsonic case, the expansion high velocity gradient does not allow the flow chemistry to relax toward equilibrium and the classic subsonic rebuilding procedure cannot be apply. Chemical non-equilibrium is also observed in arc-jets. In this case, the enthalpy characterization relies on heat transfer correlations, spectroscopic measurements, or CFD simulations.[36] In the latter method, the nozzle enthalpy is calibrated by matching the calorimeter heat flux. Similarly to ICP facilities, strong assumptions need to be made, *e.g.* to well know the catalytic efficiency of the calorimeter. Recently, efforts have been undertaken to characterize the uncertainties also for this kind of facilities.[7,47]

It is important to underline that the numerical simulation of both ICP and arc-jet is very costly. If one is interested in a deterministic simulation the computational cost is generally not a problem. Efficiency problems arise if one is interested in performing Uncertainty Quantification (UQ) studies. In this case, surrogate models, such as the Kriging,[33] are commonly used to alleviate the demanding computational cost. Anyway, they are built on training points, which are computationally expensive CFD simulations. To make the process more efficient one may leverage on a low-fidelity representation to cover much of the uncertainty space, retaining fewer high-fidelity computations to ensure accuracy.[37] Multi-fidelity approaches, such as Cokriging[15,27,29] and Hierarchical Kriging,[1,22] aims at combining these information to produce an efficient and accurate regression.

In this work, we propose a novel methodology for the Plasmatron supersonic testing characterization. The sources of uncertainties are propagated through a surrogate model trained on CFD points. The US3D solver provided a high-fidelity representation of the flow. On the one hand, this allows to achieve pronounced numerical accuracy, but, on the other hand, it makes the whole process very non-efficient. To restore efficiency, we employed a multi-fidelity strategy, whose application in the field of high enthalpy nozzle characterization is a novelty. The obtained surrogate model is verified against verification points and it is used to propagate experimental uncertainties and model unknowns. Finally, the numerically propagated uncertainties are compared to the experimental ones.
The paper is structured as follows: in Section 2) the experimental campaign is presented, in Section 3) the methodology to cost efficiently propagate the experimental/model uncertainties is proposed, in Section 4) the governing equations and the employed numeric are introduced, in Section 5) the results are illustrated, and in Section 6) the conclusion are drawn down.

2. Experimental Campaign

The VKI 1.2 MW Plasmatron facility is able to create a high enthalpy environment, which mimics the hypersonic boundary layer of an object entering the atmosphere, useful for the characterization of the material response of TPMs. It allows to explore a wide range of operative conditions, ranging from low to moderate pressure, moderate to high heat flux, and sub- to super-sonic regime. Contrary to subsonic testing, generally extensively used to duplicate entry proprieties in the stagnation point, supersonic testing allows to produce higher heat flux and, in case of an ablative sample, to provoke a non-uniform sample recession,[25] which is closer to what experienced by atmospheric entry objects. An experimental campaign was conducted to give more insights on the supersonic testing.
To achieve supersonic condition, the flow was accelerated through a sonic nozzle, mounted at the exit of the plasma torch. The chamber pressure was lowered enough to generate a highly under-expanded jet, as shown in Fig. 1. Specifically, the chamber pressure was set to 5.5 hPa, against a reservoir pressure of 165 hPa, resulting in a total pressure ratio of $\beta_0 = p_0/p_c = 30$.
The sonic nozzle has an exit diameter of 35 mm and the probe is placed at a distance of 75mm from the exit of the nozzle. The mass flux entering the plasma torch, measured through a rotameter, was set to 6 g/s, and the Plasmatron was supplied with an electrical power of 600 kW.
A 25 mm radius copper water-cooled calorimeter probe, which temperature was kept to 350 K, was used to measure the stagnation point heat flux. Furthermore, a water-cooled Pitot probe measured the Pitot pressure at the stagnation point. Their value respectively are 4.48 MW/m^2 and 25 hPa. Uncertainty on the heat flux is estimated to be the 10% of the measured value, while for pressure measurements the 0.25% of the full scale, *i.e.* 0.5 hPa. Two runs were performed to assess the repeatability of the test.
The expansion results in a complex flow structure. The numerical simulated one is shown in Fig. 2. A Prandtl-Mayer expansion fan develops at the exit of the nozzle to expand the flow from the exit nozzle pressure to the chamber one.

DOI: 10.13009/EUCASS2022-4925

The typical barrel shock allows the streamlines to align to the jet boundary. It interacts with the normal shock, caused by the interference of the probe, before the classical Mach disk is generated. After the interaction, the two shocks are transmitted. Finally the transmitted normal shock gets reflected on the jet boundary, resulting in a weak expansion fan, while the second one dissipates. These features are in good qualitative agreement with the experimental ones in Fig. 1.

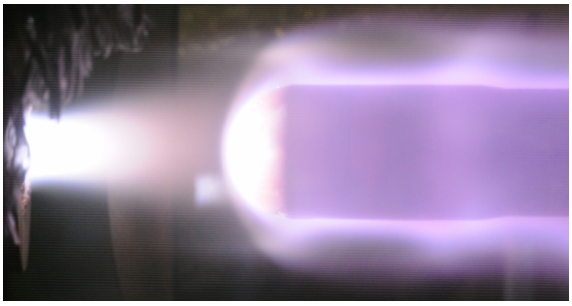

Figure 1: Under-expanded air jet over the catalytic probe.

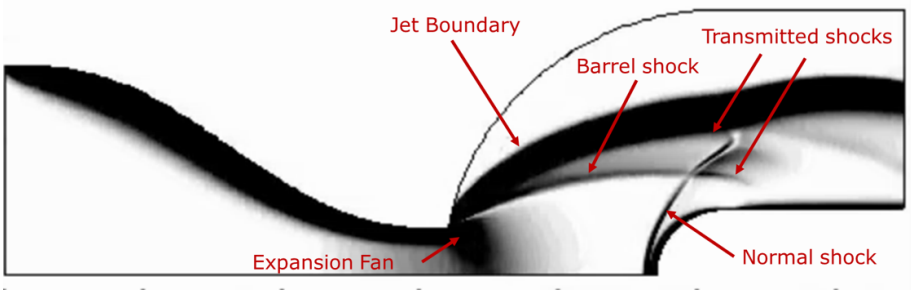

Figure 2: Numerical flow structure obtained with a total temperature of 7500 K and a total pressure of 16500 Pa imposed at the entrance of the sonic nozzle. Density gradient contours.

3. Methodology

We simulated the supersonic under-expanded jet by means of the US3D solver.[8] We chose the exit of the plasma torch as starting section for the numerical domain, as sketched in Fig. 3. This is in contrast with the procedure usually adopted for simulating the subsonic flow, where no nozzle is mounted. Its presence makes the exit torch thermo-hydrodynamic radial distribution less crucial and the inflow condition can be safely reduced to a reservoir one. Furthermore, being the flow supersonic, no characteristics travel backward from the expansion chamber to the nozzle exit. Since the plasma torch was excluded by the computational domain, it is reasonable to assume a very weak influence of the electromagnetic field: this source term will be neglected. Moreover, the flow is regarded laminar, steady, and in chemical equilibrium at the inlet. Finite rate chemistry of an air mixture of 5 species (N_2,O_2, NO, N, O) is considered in the whole domain. Finally, the surface is assumed to be partially catalytic.

The resulting computational cost is very high, and we need to restore efficiency to make the UQ problem affordable. Surrogate models, such as the Kriging,[33] are generally used to replace the CFD for a cheaper computational cost. It still requires training points, which, in the present study, come from expensive CFD simulations. Thus, the efficiency can still be improved. To this end, we made use of a multi-fidelity approach, which leverages on a low fidelity representation to explore a great part of the uncertainty space. Multi-fidelity representation, such as Cokriging[15,27,29] or Hierarchical Kriging,[1,22] are widely used in engineering problems to alleviate the prohibitive computational cost demanded by practical application.[37]

What we propose is simplified in the scheme in Fig. 4: I) the lowest fidelity (δ) is computed according to a cheap representation of the problem, which will be described in Section 4.2. The other three fidelity, γ, θ, and α, rely on the same computational model, described in Section 4.1, but made use of 3 differently refined grids, whose numerical error will be described in Section 3.3. This generally falls under the name of multi-level representation.[37] The statistical convergence is investigated by means of an adapting strategy to sample in the stochastic/fidelity space; this will be detailed in Section 3.2.

DOI: 10.13009/EUCASS2022-4925

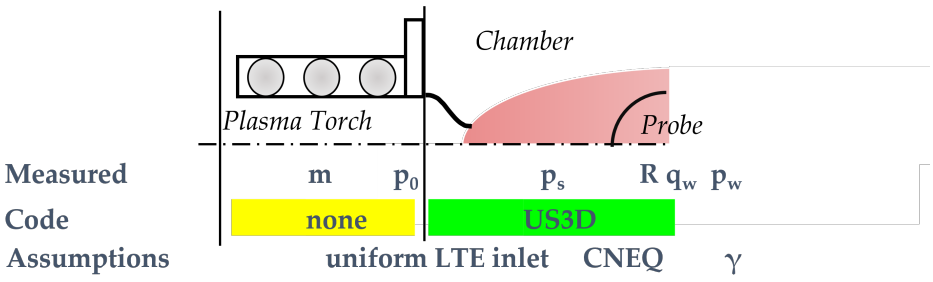

Figure 3: Sketch of the simulation.

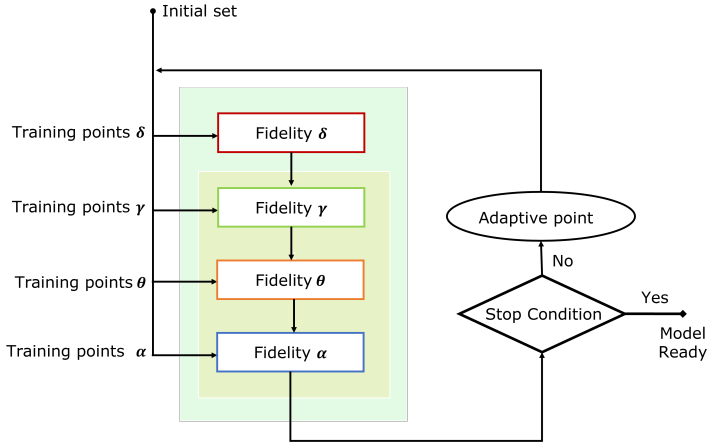

Figure 4: Scheme of the proposed hierarchical Kriging.

3.1 Hierarchical Kriging

The hierarchical Kriging, mathematically formulated by Han,[22] proposes to exploit the $l-1$ fidelity prediction ($\hat{\mathcal{Y}}_{l-1}(\mathbf{x})$), scaled by a β_l parameter, as trend function for the l fidelity Kriging:

$$Y_l(\mathbf{x}) = \beta_l \hat{\mathcal{Y}}_{l-1}(\mathbf{x}) + Z_l(\mathbf{x}) \tag{1}$$

After conditioning the Gaussian process on n_l training points and optimizing the model hyperparameters, the l fidelity predictor, $\hat{\mathcal{Y}}_l(\mathbf{x})$, is obtained. An exhaustive description of the formulation, avoided for concision here, can be find in the work of Han.[22] Its main advantages are:

- Efficiency and implementation ease: it does not require a cross correlation function to be built, as for cokriging modeling; being one Kriging evaluated per fidelity it demands the inversion of l correlation matrix of size $n_l \times n_l$ in spite of a $(l \cdot n_l) \times (l \cdot n_l)$ matrix, which is advantageous for computer performing.
- Training points independence: the set of lower fidelity training points does not require the inclusion of the high fidelity ones.
- Infill techniques easily applicable: its Gaussian variance is well suited for adaptive sampling.

The surrogate model was built by means of the software UQLAB,[32] where the hierarchical Kriging implementation is very straightforward.[1,31]

3.2 Adapting Sampling Strategy

Adaptive strategy allows to iteratively sample from the stochastic space a new training point to improve the quality of the surrogate model.[16] When one deals with optimization problems, one is interested to exploit the already existing surrogate model, and its associate Gaussian variance, to locally refine the model in points that are candidates to be

DOI: 10.13009/EUCASS2022-4925

minima or *maxima*. Among these *exploiting* methods, the Expected Improvement, proposed by Jones,[28] and its variations[38] are widely used examples. Contrary to this, *exploring* strategies are used to globally increase the quality of the surrogate model. Since our interest is to adaptively improve the overall quality of the model, we rely on *exploring* strategies. Gaussian processes are very suitable for this, as they are characterized by a process variance, which in a nutshell measures how uncertain we are on the prediction on a given untrained point. It thus make sense to sample where this uncertainty is the highest. When it comes to multi fidelity representation, we are not only interested in sampling in the stochastic space, but we also want to have a criteria to establish which fidelity level we want to refine. In this study, we slightly modified the strategy proposed by Zhang.[50] Since the low fidelity prediction is scaled by a β factor, the low fidelity uncertainty should be scaled by the same factor, such that:

$$s^2(\mathbf{x}, l) = \begin{cases} \beta_{hf}^2 s_{lf}^2(\mathbf{x}) & \text{if l = low fidelity} \\ s_{hf}^2(\mathbf{x}) & \text{if l = high fidelity} \end{cases}, \tag{2}$$

where s^2 is the Gaussian variance. Zhang's work refers to an optimization problem, so the Expected Improvement (EI) was maximized:

$$(\mathbf{x}, l) = \text{argmax } EI_{vf}(\mathbf{x}, l). \tag{3}$$

Contrary, in the present work, we want to rely on more than 2 fidelity models, and adaptively exploring the high fidelity one. Following Zhang's work, it makes sense to scale the l fidelity variance, by the products of the l scaling factors that separates it from the high fidelity one:

$$s^2(\mathbf{x}, l) = \begin{cases} (\prod_{i=l+1}^{HF} \beta_i^2) s_l^2(\mathbf{x}) & \text{if l} \neq \text{high fidelity} \\ s_{hf}^2(\mathbf{x}) & \text{if l = high fidelity} \end{cases} \tag{4}$$

Furthermore, for exploring purposes, we want to train where the the standard deviation is maximum:

$$(\mathbf{x}, l) = \text{argmax } s(\mathbf{x}, l) \tag{5}$$

3.3 Numerical uncertainty

To determine the numerical error associated to a given meh, we followed the procedure proposed by Eça.[12] It reads:

$$\epsilon_\phi \approx \delta_{\text{RE}} = \phi_{\text{i}} - \phi_0 = \alpha h_{\text{i}}^p. \tag{6}$$

The quantity ϕ_{i} is a flow quantity of interest at the grid refinement i, ϕ_0, the estimate of the exact solution, α, a constant to be determined, h_{i}, the typical cell size and p is the observed order of grid convergence. In most of the application the exact solution of the quantity of interest cannot be analytically computed; in these cases, it can be estimate as asymptotic limit for the element size approaching the infinitesimal value. Hence, the QoI at the refinement i can be approximated as:

$$\phi_{\text{i}} = \phi_0 + \alpha h_{\text{i}}^p. \tag{7}$$

By using a minimum of four nested meshes, the values α, p, and ϕ_0 can be estimate by minimizing the standard deviation, σ, between the numerical solutions and the fit law (Eq. (7)). A positive value of order of convergence (p) implies a monotonic convergence, in contrast a negative value a monotonic divergence.
Still according to Eça, the uncertainty on the prediction associated to the mesh at the refinement i reads:

$$U_\phi(\phi_{\text{i}}) = \begin{cases} F_{\text{s}} \epsilon_\phi(\phi_{\text{i}}) + \sigma + |\phi_{\text{i}} - \phi_{\text{fit}}|, & \text{if } \sigma < \Delta_\phi \\ 3\frac{\sigma}{\Delta_\phi}(\epsilon_\phi(\phi_{\text{i}}) + \sigma + |\phi_{\text{i}} - \phi_{\text{fit}}|), & \text{otherwise} \end{cases} \tag{8}$$

where $\Delta\phi = (\phi_{\text{i}}^{\max} - \phi_{\text{i}}^{\min})/(n_g - 1)$ is a data range parameter and F_s is a safety factor equal to 1.25 if $0.5 < p < 2.1$ and $\sigma < \Delta\phi$, and to 3 otherwise.

4. Governing Equations and Numerical Set-up

We simulated the gas expansion from the beginning of the sonic nozzle. Here the influence of the magnetic field is negligible and we can correctly describe the flow using the only Navier-Stokes equations. For a mixture of n_s chemical reacting species in thermal equilibrium, they read:

$$\frac{\partial \rho_{\text{i}}}{\partial t} + \nabla \cdot (\rho_{\text{i}} \mathbf{u} + \mathbf{j}_{\text{i}}) = \dot{\omega}_{\text{i}}, \quad \forall \text{i} \in S, \tag{9}$$

DOI: 10.13009/EUCASS2022-4925

$$\frac{\partial \rho \mathbf{u}}{\partial t} + \nabla \cdot (\rho \mathbf{u} \cdot \mathbf{u} + p\bar{\bar{\mathrm{I}}} + \bar{\bar{\tau}}) = \mathbf{0}, \tag{10}$$

$$\frac{\partial \rho E}{\partial t} + \nabla \cdot (\rho \mathbf{u} H + \bar{\bar{\tau}}\mathbf{u} + \mathbf{q}) = 0. \tag{11}$$

Symbol S stands for the set of species indices, ρ_i is the partial density of species i, $\mathbf{u}$ is the mass-averaged mixture velocity, $\mathbf{j}_\mathrm{i}$ the diffusion mass flux of species i, $\dot{\omega}_\mathrm{i}$ its chemical production/destruction rate, p, the thermodynamic pressure of the mixture, $\bar{\bar{\tau}}$, the viscous stress tensor, E, the total energy, $H = E + p/\rho$, the total enthalpy, and $\mathbf{q}$, the total heat flux. Thermodynamics properties are obtained using the NASA polynomials.[19] Diffusion mass fluxes are computed using the self-consistent effective binary diffusion models,[39] while viscosity and thermal conductivity are computed according to Gupta-Yos mixing rule.[21] Chemical production rates $\dot{\omega}_\mathrm{i}$ for species i are computed using finite-rate chemistry with rate coefficients taken from Park.[35]

The probe acts as a catalyst for the recombination of atomic nitrogen and oxygen impinging to its surface. The recombination reaction is exothermic and its contribute to the total heat flux must be taken into account. The set of surface reactions and heat exchange can be numerically expressed as a boundary condition. It returns to the CFD solver the surface state computed by solving balance equations in an infinitesimal volume containing both the gas and material phases. In this study, this BC was provided through MUTATION^{++}.[5,9,43]

When the surface temperature is known (isothermal condition) the wall composition can be obtained by solving the surface mass balance for each species i, which for a catalytic material reads:

$$\dot{\omega}_\mathrm{i} = \mathbf{j}_\mathrm{i} \cdot \mathbf{n}, \quad \forall \mathrm{i} \in S. \tag{12}$$

Versor $\mathbf{n}$ is the normal to the surface. The system (12) is solved by means of a Newton method and the surface state is returned to the CFD solver. In this work we used a phenomenological approach[20] to describe the chemical source term. It is widely used in the hypersonic community because of their simplicity and it only requires the definition of the probability that a macroscopic reaction takes place:

$$\gamma_\mathrm{i}^{rea} = \frac{\mathcal{N}_\mathrm{i}^{rea}}{\mathcal{N}_\mathrm{i}}, \tag{13}$$

where $\mathcal{N}_\mathrm{i}^{rea}$ is the number flux of species i subject to the reaction and $\mathcal{N}_\mathrm{i} = n_\mathrm{i}\sqrt{k_\mathrm{b}T_\mathrm{s}/(2\pi m_\mathrm{i})}$, the number flux of species i impinging the surface. Symbol k_b stands for Boltzmanns constant, T_s the surface temperature, and m_i, the mass of species i. A fully catalytic behavior is obtained when the probability approaches unity; whereas a non-catalytic behavior is reached when is equal to zero. The chemical production rate reads:

$$\dot{\omega}_\mathrm{i}^\mathrm{s} = m_\mathrm{i}\gamma_\mathrm{i}^{rea}\mathcal{N}_\mathrm{i}. \tag{14}$$

The two previously mentioned fidelity models are described next: I) the high fidelity US3D solver, described in Section 4.1 and II) a low fidelity model which is described in Section 4.2.

4.1 High fidelity model

To build the high fidelity surrogate model we employed the software US3D. It is a three-dimensional finite-volume flow solver developed at the University of Minnesota for aerodynamic/hypersonic applications.[8] In this work we computed the numerical fluxes according to the modified Steger-Warming scheme[44] with a MUSCL approach to obtain second-order accuracy. The Data Parallel Line Relaxation (DPLR[49]) was used to obtain rapid convergence to steady-state. The solver is highly scalable and efficient, making it possible to solve very large problems on parallel computers in a cost-effective manner.

The physical domain was discretized as shown in Fig. 5(a); from the left, in a clockwise direction, we can see the I) exit of plasma torch/nozzle inlet, II) sonic nozzle surface, III) expansion chamber, and IV) probe. Particular attention was posed to well capture the shock to have reliable results on the probe surface: as one can see in Fig. 5(b) the grid is aligned to the shock and the cells are stretched in the shock direction.

Four grids, listed on table 1, are obtained by systematically doubling the number of the nodes in the both the x and y directions to assess the grid convergence.

Total temperature and pressure were imposed at the nozzle inlet and the chemical composition was assumed to be at equilibrium. Their values were set according to the training points. The nozzle surface was characterized by an isothermal condition (whose temperature was kept constant at 1500 K for all the simulations). The chamber free surface was characterized by an inlet condition for numerical stability; it is characterized by a small velocity (1 m/s),

DOI: 10.13009/EUCASS2022-4925

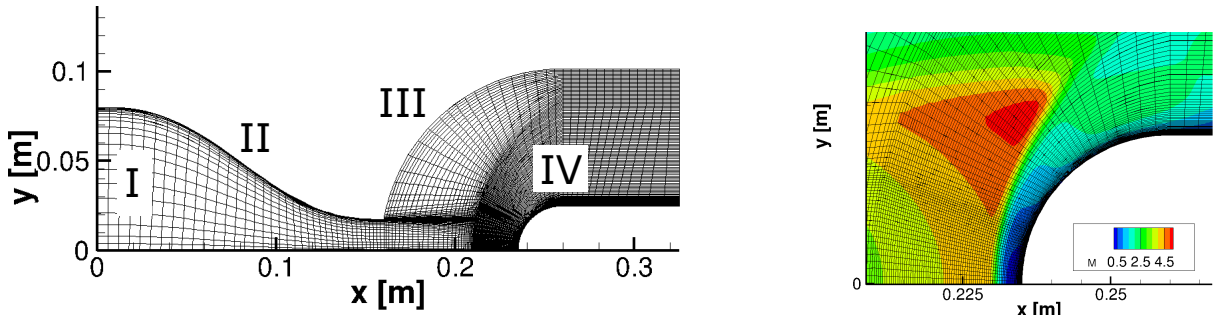

(a) Numerical domain, from the left, in the clockwise direction: I) exit of plasma torch/nozzle inlet, II) sonic nozzle surface, III) expansion chamber and IV) probe.

(b) Zoom of the numerical domain: grid aligned to the shock and stretched in the direction of the shock.

Figure 5: Details of mesh III on table 1.

Table 1: Used meshes: index, number of cells, length of first cell on the stagnation point (Δx), normalized characteristic mesh, h_i, time to converge, t_{CPU}.

Tag	cells	Δx [m]	h_i	t_{CPU} [min]
I	172224	5E-7	1	$\approx$ 1600
II	43056	1E-6	2	$\approx$ 200
III	10764	2E-6	4	$\approx$ 30
IV	2691	4E-6	8	$\approx$ 4

room temperature and a chamber pressure of 5.5 hPa (also these conditions were kept constant for all the simulations). The probe was modeled as an isothermal/catalytic surface with a temperature of 350K and a recombination probability that was changed according to the training points. Finally, all the other surfaces were characterized by a symmetry boundary condition.
A nominal condition (T_0 = 7500 K, p_0 = 16500 Pa, γ_N = 0.0736, and γ_O = 0.1170) was imposed to characterize the numerical uncertainty, based on the formulation proposed in Section 3.3, and on the four meshes reported on table 1. The results for the stagnation point pressure and heat flux, and for the nozzle mass flux are reported on table 2. The mesh I numerical uncertainty is lower than the experimental one for all the QoI, making it a very accurate representation. Anyway the coarser meshes, even if not as well accurate, can be employed to enrich the stochastic space in a multi-level fashion.

Table 2: Results of the convergence study performed on the meshes on Table 1 for each QoI: order of convergence, p, asymptotic value, ϕ_0, numerical uncertainty of grid I on table 1, U_1, and experimental uncertainty, U_{exp}.

QoI	p	ϕ_0 [as QoI]	U_1 [as QoI]	U_{exp} (95 %) [as QoI]
p [Pa]	1.57	2426.90	38.57	50
q [W/m^2]	1.57	4.48E6	7.5E4	4.48E5
m [kg/m^2/s]	0.55	5.8E-3	1.1E-4	3E-4

4.2 Low Fidelity Model

To further speed up the building process, a low fidelity representation of the gas expansion was built. Firstly, nozzle area equations were used to compute the state of the gas just before the shock. The geometrical throat area, together with the assumption of $M = 1$ at the exit of the nozzle, constant h_0 and p_0, and chemistry frozen allows to compute the nozzle choked mass flux and exit gas state, for a given reservoir condition. From here, we can compute the state just before the shock imposing the previously computed mass flux and the total enthalpy and pressure conservation. The jet diameter before the shock was imposed as function of the reservoir pressure, which law was calibrated using 3 mesh IV computations. By means of the same computations, it was also inferred a law for the velocity gradient ($\beta = \partial v/\partial y$). These values, together with the gas state, served as input to an in-house software,[34] which solves equation along the

DOI: 10.13009/EUCASS2022-4925

stagnation line. Output of the whole procedure are the stagnation point pressure and heat flux.

5. Results

5.1 Nominal results

The results presented in this section refer to a nominal total temperature of 7500 K and a total pressure of 16500 Pa imposed at the entrance of the sonic nozzle, and a nitrogen recombination probability of 0.0736 and oxygen of 0.1170 assign to model surface catalytic activity. The numerical flow structure obtained with the finest grid (mesh I on table 1), already discussed in Section 2 is plotted in Fig. 2. Being the total pressure ratio, $\beta_0 = p_0/p_c = 30$, very high, we retrieve some of the compressible features typical of an extremely under-expanded jet,[17] namely: I) Prandtl-Mayer expansion fan, II) jet boundary, III) barrel shock IV) normal shock, and V) transmitted shocks. A zoom in the shock region is given in Fig. 6: the shock is attached to the BL (its stand-off distance, taken at the location of half of the temperature jump, is 3.9 mm) and it results to be very diffused (3 mm of extension). Similar flow patterns were observed by Gordeev and Sakharov[18,40] for the simulation of an experiments conducted with the VGU-4 induced plasmatron of the Institute for Problems in Mechanics of the Russian Academy of Sciences in similar operative conditions (P_{el}=45 kW, $\dot{m}$ = 3.6 g/s and P_c=8.5 hPa). We remark that while they conducted their analysis focusing on investigating the evolution of heat flux and pressure along the center line for different cases in a deterministic manner, we pose attention into the characterizing of the uncertainties to well establish the experiments conditions.
It is also worth to analyze the chemistry of the flow: nitrogen and oxygen mass fractions, and temperature profile are plotted in Fig. 7 along the central line, from the nozzle entrance to the probe stagnation point. The fast expansion does not allow the chemistry to relax, resulting in a nearly frozen flow up to the edge of the boundary layer, where atoms recombine, mostly driven by surface catalysis.

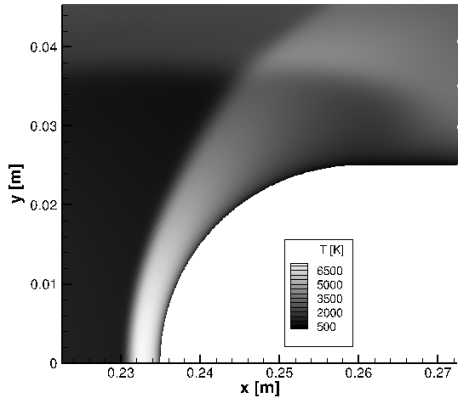

Figure 6: Numerical shock stand-off distance obtained in nominal condition: 3.9 mm at half of the temperature jump.

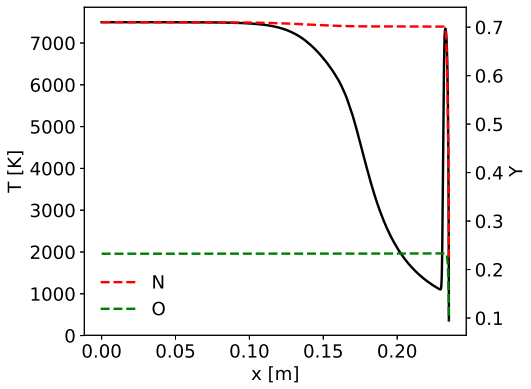

Figure 7: Temperature and mass fractions along the center line, from the nozzle inlet to the probe.

5.2 Uncertainty Propagation

The total pressure at the entrance of the nozzle was measured, thus we assigned a Gaussian distribution to this variable: its mean and confidence intervals are given on table 3. On the other hand, the total temperature was not measured and it was characterized by a non informative uniform distribution. The presented uncertainty is a reduced support of the one used to build the surrogate model: only the range leading to a correct mass flux was retained. The nominal recombination efficiencies were taken from the work of Bellas,[4] who computed them applying, for a similar surface condition, the finite rate chemistry model proposed by Barbato.[3] A 20% uninformative uncertainty was applied.
A number of 80 training points were selected for the low fidelity model (fidelity δ); this allows to cover much of the uncertainty space very cost efficiently. From the high fidelity representation, 3 numerical grids, namely I, III, IV, were chosen, in a multi-level framework, to characterize the fidelity α, θ, and γ. Other 5 training points were sampled for

DOI: 10.13009/EUCASS2022-4925

Table 3: List of propagated uncertainties.

Variable	Mean	Minimum	Maximum	Distribution
p_0 [Pa]	16500	16000	17000	Gaussian
T_0 [K]	6900	6400	7400	Uniform
γ_N [-]	0.075	0.06	0.09	Uniform
γ_O [-]	0.12	0.096	0.144	Uniform

each of these fidelity. Further 5 independent α points were computed for verification purposes.
A number of 17 new training points were sampled for the fidelity γ and 13 for the fidelity θ, by means of the adaptive strategy proposed in Section 3.2. As one can see from Fig. 8, most of these points tend to be selected close to the boundaries, as one would expect when employing an exploring infill criteria. The resulting normalized error NRMSE, defined in Eq. (15), is below the 0.5% for all the QoI. The QQplots for the multi-fidelity approach (in blue) and for the Kriging built on the only high fidelity points relative to the heat flux (in red) is plotted in Fig. 9: it is evident the gain in accuracy when the multi fidelity is used.

$$NRMSE = \sqrt{\frac{\sum_{i=0}^{N_v}(Y_{v,i} - \hat{Y}_i)^2}{N_v}} \frac{100}{\overline{\hat{Y}}}. \tag{15}$$

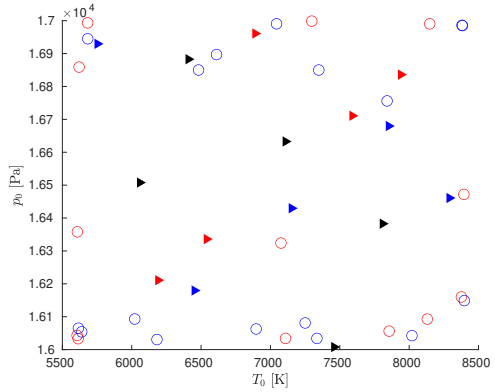

Figure 8: Training points projections; triangles for the original LHS samples, circle for added points. In black fidelity α, in red fidelity θ, and in blue fidelity γ.

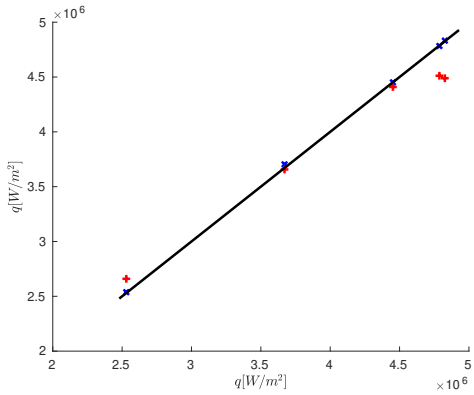

Figure 9: QQplot of the heat flux. Multi fidelity values in blue. Kriging on the only high fidelity points in red.

The verified surrogate model was used to propagate uncertainties by means of a Monte Carlo method. The obtained probabilistic density functions are plotted in Fig. 10. The numerical density function (in red) for each QoI is plotted against the experimental one (in blue). The temperature confidence interval was chosen to produce a good superimposition of the numerical and experimental mass flux confidence intervals. When this condition is met, pressure and heat flux partially superimpose. A Bayesian approach, foreseen as future work, will allow to determine the most probable reservoir state for a complete characterization.

6. Conclusion

A methodology for the characterization of an under-expanded supersonic flow over a catalytic probe was proposed: the experimental/modeling uncertainties were propagated through a surrogate model. We have shown that multi-fidelity strategies can reasonably be employed in this context to improve the efficiency of the numerical effort. The surrogate model was verified and used to propagate the uncertainties. The relative probabilistic distribution of all the quantities of interest result to partially overlap with the experimental one.
As future work we propose to infer the reservoir condition, as well as the catalytic proprieties of the probe, in a Bayesian framework.

DOI: 10.13009/EUCASS2022-4925

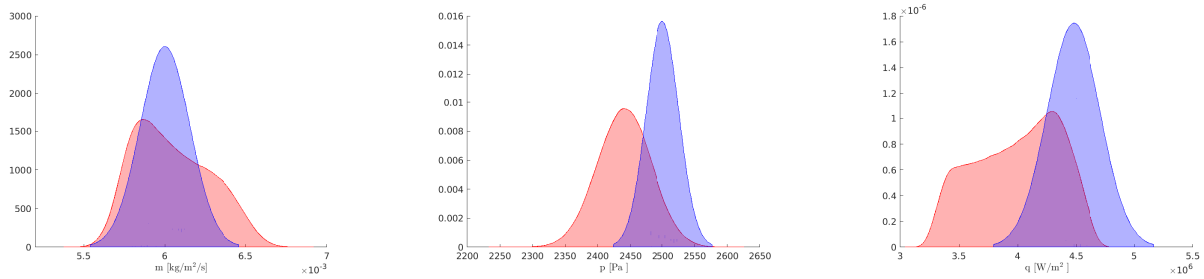

(a) Mass flux. (b) Pressure. (c) Heat flux.

Figure 10: Probabilistic density functions for each QoI. Red area from the numerical propagation and blue area values from the experiments

7. Acknowledgments

Authors acknowledge the Air Force Office of Scientific Research (AFOSR) for supporting the work under the grant FA9550-18-1-0209.

References

[1] Imad Abdallah, Christos Lataniotis, and Bruno Sudret. Parametric hierarchical kriging for multi-fidelity aero-servo-elastic simulators ăApplication to extreme loads on wind turbines. *Probabilistic Engineering Mechanics*, 55:67–77, 2019.

[2] John Balboni, Samuel A. Cohen, and Tobin Munsat. Arc jets for divertor component testing. *Journal of Nuclear Materials*, 241-243:483–488, 02 1997.

[3] M. Barbato, S. Reggiani, C. Bruno, and J. Muylaert. Model for heterogeneous catalysis on metal surfaces with applications to hypersonic flows. *Journal of Thermophysics and Heat Transfer*, 14(3):412–420, 2000.

[4] "G. Bellas-Chatzigeorgis". *"Development of advanced gas-surface interaction models for chemically reacting flows for re-entry conditions"*. PhD thesis, Politecnico di Milano, 2001.

[5] Georgios Bellas Chatzigeorgis, Alessandro Turchi, Alan Viladegut, Olivier Chazot, Paolo Francesco Barbante, and Thierry Magin. Development of catalytic and ablative gas-surface interaction models for the simulation of reacting gas mixtures. In *23rd AIAA Computational Fluid Dynamics Conference*. American Institute of Aeronautics and Astronautics, 2017.

[6] Benoit Bottin, Olivier Chazot, Mario Carbonaro, V. Haegen, and S. Paris. The VKI Plasmatron Characteristics and Performance. page 26, 04 2000.

[7] Andrew J. Brune, Thomas K. West, and Laura M. White. Calibration Probe Uncertainty and Validation for the Hypersonic Material Environmental Test System. *Journal of Thermophysics and Heat Transfer*, 34(2):404–420, 04 2020.

[8] Graham V. Candler, Heath B. Johnson, Ioannis Nompelis, Vladimyr M. Gidzak, Pramod K. Subbareddy, and Michael Barnhardt. Development of the US3D Code for Advanced Compressible and Reacting Flow Simulations. In *53rd AIAA Aerospace Sciences Meeting*. American Institute of Aeronautics and Astronautics, 2015.

[9] M. Capriati, K. Prata, T. Schwartzentruber, G. Candler, and T. Magin. Development of a nitridation gas-surface boundary condition for high-fidelity hypersonic simulations. In *14th WCCM-ECCOMAS Congress*. CIMNE, 2021.

[10] Anabel del Val, Olivier P. Le Maître, Thierry E. Magin, Olivier Chazot, and Pietro M. Congedo. A surrogate-based optimal likelihood function for the Bayesian calibration of catalytic recombination in atmospheric entry protection materials. *Applied Mathematical Modelling*, 101:791–810, 2022.

[11] Anabel del Val, Diana Luis, and Olivier Chazot. Experimental methodology for the accurate stochastic calibration of catalytic recombination affecting reusable spacecraft thermal protection systems. 12 2021.

DOI: 10.13009/EUCASS2022-4925

[12] L. Eça and M. Hoekstra. A procedure for the estimation of the numerical uncertainty of CFD calculations based on grid refinement studies. *Journal of Computational Physics*, 262:104–130, 2014.

[13] Andrea Fagnani, Bruno Dias, Pierre Schrooyen, Bernd Helber, Thierry E. Magin, and Olivier Chazot. Investigation of Quartz Ablation in the VKI Plasmatron Facility: Comparison Between Experimental and Numerical Results. In *AIAA AVIATION 2021 FORUM*. American Institute of Aeronautics and Astronautics, 08 2021.

[14] Andrea Fagnani, Damien Le Quang Huy, Bernd Helber, Simon Demange, Alessandro Turchi, Olivier Chazot, and Annick Hubin. Investigation of a Free-Stream Air Plasma Flow by Optical Emission Spectroscopy and Comparison to Magnetohydrodynamics Simulations. In *AIAA Scitech 2020 Forum*. American Institute of Aeronautics and Astronautics, 01 2020.

[15] Alexander Forrester, Andras Sobester, and Andy Keane. Multi-fidelity optimization via surrogate modelling. *Proc. R. Soc. A*, 463:3251–3269, 12 2007.

[16] Alexander Forrester, Andras Sobester, and Andy Keane. *Engineering Design via Surrogate Modelling: A Practical Guide*. Wiley, 2008.

[17] Erwin Franquet, Vincent Perrier, Stéphane Gibout, and Pascal Bruel. Review on the underexpanded jets. 09 2015.

[18] A. N. Gordeev, A. F. Kolesnikov, and V. I. Sakharov. Experimental and Numerical Investigation of Heat Exchange between Underexpanded High-Enthalpy Air Jets and Cylindrical Models. *Fluid Dynamics*, 53(5):702–710, September 2018.

[19] S. Gordon and J. McBride. Thermodynamic Data to 20,000 K For Monatomic Gases. Technical Report 1999-208523, NASA, 1999.

[20] R. Goulard. On Catalytic Recombination Rates in Hypersonic Stagnation Heat Transfer. *Journal of Jet Propulsion*, 28(11):737–745, 1958.

[21] R.N. Gupta, J.M. Yos, R.A. Thompson, and K. Lee. A Review of Reaction Rates and Thermodynamic and Transport Properties for an 11-Species Air Model for Chemical and Thermal Nonequilibrium Calculations to 30000K. *NASA R. P 1232*, 1990.

[22] Zhong-Hua Han and Stefan Görtz. Hierarchical kriging model for variable-fidelity surrogate modeling. *AIAA Journal*, 50(9):1885–1896, 2012.

[23] Bernd Helber, Olivier Chazot, Annick Hubin, and Thierry E. Magin. Microstructure and gas-surface interaction studies of a low-density carbon-bonded carbon fiber composite in atmospheric entry plasmas. *Composites Part A: Applied Science and Manufacturing*, 72:96–107, 2015.

[24] Bernd Helber, Olivier Chazot, T. Magin, and Annick Hubin. *Space and Time-Resolved Emission Spectroscopy of Carbon Phenolic Ablation in Air and Nitrogen Plasmas*. American Institute of Aeronautics and Astronautics, 06 2013.

[25] Bernd Helber, Alessandro Turchi, Olivier Chazot, Thierry E. Magin, and Annick Hubin. *Gas/Surface Interaction Study of Low-Density Ablators in Sub- and Supersonic Plasmas*. American Institute of Aeronautics and Astronautics, 06 2014.

[26] Bernd Helber, Alessandro Turchi, and Thierry E. Magin. Determination of active nitridation reaction efficiency of graphite in inductively coupled plasma flows. *Carbon*, 125:582–594, 2017.

[27] R. J. Howarth. Mining Geostatistics. *Mineralogical Magazine*, 43(328):563564, 1979.

[28] Donald Jones, Matthias Schonlau, and William Welch. Efficient Global Optimization of Expensive Black-Box Functions. *Journal of Global Optimization*, 13:455–492, 12 1998.

[29] M. C. Kennedy and A. O'Hagan. Predicting the Output from a Complex Computer Code When Fast Approximations Are Available. *Biometrika*, 87(1):1–13, 2000.

[30] A. F. Kolesnikov. Conditions of simulation of stagnation point heat transfer from a high-enthalpy flow. *Fluid Dynamics*, 28:131–137, 1993.

DOI: 10.13009/EUCASS2022-4925

[31] Christos Lataniotis, Stefano Marelli, and Bruno Sudret. The Gaussian Process Modeling Module in UQLab. 05 2018.

[32] Stefano Marelli and Bruno Sudret. UQLab: A Framework for Uncertainty Quantification in Matlab. In *Vulnerability, Uncertainty, and Risk*, pages 2554–2563. American Society of Civil Engineers, 2014.

[33] G. Matheron. Principles of geostatistics. *Economic Geology*, 58:1246–1266, 1963.

[34] A. Munafò and T. E. Magin. Modeling of stagnation-line nonequilibrium flows by means of quantum based collisional models. *Physics of Fluids*, 26(9):097102, 2014.

[35] Chul Park, Richard L. Jaffe, and Harry Partridge. Chemical-Kinetic Parameters of Hyperbolic Earth Entry. *Journal of Thermophysics and Heat Transfer*, 15(1):76–90, 2001.

[36] Chul Park, George A. Raiche, David M. Driver, Joseph Olejniczak, Imelda Terrazas-Salinas, T. Mark Hightower, and Takeharu Sakai. Comparison of Enthalpy Determination Methods for an Arc-Jet Facility. *Journal of Thermophysics and Heat Transfer*, 20(4):672–679, 10 2006.

[37] Benjamin Peherstorfer, Karen Willcox, and Max Gunzburger. Survey of Multifidelity Methods in Uncertainty Propagation, Inference, and Optimization. *SIAM Review*, 60(3):550–591, 2018.

[38] Victor Picheny, Tobias Wagner, and David Ginsbourger. A benchmark of kriging-based infill criteria for noisy optimization. *Structural and Multidisciplinary Optimization*, 48, 09 2013.

[39] J. D. Ramshaw and C. H. Chang. Ambipolar diffusion in two-temperature multicomponent plasmas. *Plasma Chemistry and Plasma Processing*, 13(3):489–498, 09 1993.

[40] V. I. Sakharov. Numerical simulation of thermally and chemically nonequilibrium flows and heat transfer in underexpanded induction plasmatron jets. *Fluid Dynamics*, 42(6):157–168, 2007.

[41] Francois Sanson, P.M. Congedo, N. Villedieu, Olivier Chazot, Thierry Magin, and Francesco Panerai. Quantification of uncertainty on the catalytic property of reusable thermal protection materials from high enthalpy experiments. *Experimental Thermal and Fluid Science (EXP THERM FLUID SCI)*, 82, 12 2016.

[42] Francois Sanson, Francesco Panerai, Thierry Magin, and P.M. Congedo. Robust reconstruction of the catalytic properties of thermal protection materials from sparse high-enthalpy facility experimental data. *Experimental Thermal and Fluid Science*, 96, 03 2018.

[43] James B. Scoggins, Vincent Leroy, Georgios Bellas-Chatzigeorgis, Bruno Dias, and Thierry E. Magin. Mutation + + : MUlticomponent Thermodynamic And Transport properties for IONized gases in C++. *SoftwareX*, 12:100575, 2020.

[44] Joseph L Steger and R.F Warming. Flux vector splitting of the inviscid gasdynamic equations with application to finite-difference methods. *Journal of Computational Physics*, 40(2):263–293, 1981.

[45] Alessandro Turchi, Juan J. Matesanz Saiz, Thierry Magint, and Olivier Chazot. Duplication of hypersonic stagnation-region aerothermochemistry and gas-surface interaction in high-enthalpy ground testing. *Experiments in Fluids*, 62, 2021.

[46] Anabel del Val, Olivier P. Le Maître, Olivier Chazot, Pietro M. Congedo, and Thierry E. Magin. Inference Methods for Gas-Surface Interaction Models: From Deterministic Approaches to Bayesian Techniques. In Massimiliano Vasile and Domenico Quagliarella, editors, *Advances in Uncertainty Quantification and Optimization Under Uncertainty with Aerospace Applications*, volume 8, pages 349–364. Springer International Publishing, 2021. Series Title: Space Technology Proceedings.

[47] Patricia Ventura Diaz, Almudena Parente, Jeremie B. Meurisse, Steven Yoon, and Nagi Mansour. High-Fidelity Numerical Analysis of Arc-Jet Aerothermal Environments. In *AIAA Scitech 2020 Forum*. American Institute of Aeronautics and Astronautics, 01 2020.

[48] A. Viladegut and O. Chazot. Empirical Modeling of Copper Catalysis for Enthalpy Determination in Plasma Facilities. *Journal of Thermophysics and Heat Transfer*, 34(1):26–36, 2020.

[49] Michael J. Wright, Graham V. Candler, and Deepak Bose. Data-Parallel Line Relaxation Method for the Navier-Stokes Equations. *AIAA Journal*, 36(9):1603–1609, 1998.

DOI: 10.13009/EUCASS2022-4925

[50] Yu Zhang, Zhong-Hua Han, and ke-shi Zhang. Variable-fidelity expected improvement method for efficient global optimization of expensive functions. *Structural and Multidisciplinary Optimization*, 58, 10 2018.